The effect of wood composition and supercritical CO2 extraction on charcoal production in ferroalloy industries

Gerrit Ralf Surup, Andrew J. Hunt, Thomas M. Attard, Vitaliy L. Budarin, Fredrik Forsberg, Mehrdad Arshadi, Victor Abdelsayed, Dushyant Shekhawat, Anna Trubetskaya

The effect of wood composition and supercritical CO_2 extraction on charcoal production in ferroalloy industries

Gerrit Ralf Surup[a], Andrew J Hunt[b], Thomas Attard[c], Vitaliy L Budarin[c], Fredrik Forsberg[d], Mehrdad Arshadi[e], Victor Abdelsayed[f,g], Dushyant Shekhawat[f], Anna Trubetskaya[h,*]

[a]*Department of Materials Science and Engineering, Norwegian University of Science and Technology, 7491, Trondheim, Norway*

[b]*Materials Chemistry Research Center, Department of Chemistry and Center of Excellence for Innovation in Chemistry, Faculty of Science, Khon Kaen University, 123 Mittraparb Road, 40002, Khon Kaen, Thailand*

[c]*Department of Chemistry, The University of York, Heslington, York, YO10 5DD, UK*

[d]*Department of Engineering Sciences and Mathematics, Luleå University of Technology, 97187, Luleå, Sweden*

[e]*Department of Forest Biomaterials and Technology, Swedish University of Agricultural Sciences, 90183, Umeå, Sweden*

[f]*National Energy Technology Laboratory, Morgantown, WV 26507, USA*

[g]*Leidos Research Support Team, Morgantown, WV 26507, USA*

[h]*Department of Chemical Sciences, University of Limerick, V94 T9PX, Limerick, Ireland*

Abstract

This work demonstrates that the integration of supercritical carbon dioxide extraction with slow pyrolysis is an effective method for the production of value-added chemicals and charcoal that is an attractive alternative to coke for industry. Integration of technologies is key for the development of holistic biorefineries that exploit all parts of the biomass feedstock and generate little or ideally no waste. In fact, the use of waste or low valued wood fractions is attractive due to their plentiful abundance and lack of exploitation.

*Corresponding author. anna.trubetskaya@ul.ie

Supercritical carbon dioxide has been demonstrated to be effective at the removal of over half of extractives from low quality wood and forestry wastes, which can account for up to 11 wt. %, of the dried biomass in waste needles. High extractive yields by supercritical carbon dioxide extraction illustrates the potential of utilizing low quality wood as an alternative feedstock for the sustainable production of value-added chemicals. High yields of steroids and derivatives, terpenes and other plant metabolites were obtained in the extracts of needles, branches and bark. Importantly, supercritical carbon dioxide extraction had little impact neither on the physical properties of original wood nor on the yield of solid charcoal. This indicates that extraction by supercritical carbon dioxide can be used as a method for adding further value to the process by removal of bio-based chemicals, whilst still maintaining the yield of the solid fuel product. Moreover, the heat treatment temperature and supercritical carbon dioxide extraction had a significant impact on the tar yields during pyrolysis, leading to an increase in naphthalene, polycyclic aromatic hydrocarbons, aromatic and phenolic fractions with greater temperature. These results are promising as they show that the charcoal obtained from this renewable feedstock could be used as an alternative to fossil-based coke in applications including ferroalloy industries.
Keywords: biorefinery, pyrolysis, supercritical, sterols, solid fuels

1. Introduction

Wood for energy purposes represents about 9 % of the total wood utilization in Sweden [1, 2]. Pelletized softwood such as Scots pine and Norway spruce are major solid feedstocks for energy production in Sweden [2]. The

separation of extractives from the wood provides a valuable feedstock for the energy sector and metallurgical industries [3]. The extracted fatty/resin acids can be utilized as primary feedstocks for chemicals and biorefinery applications [4–7], whereas the wood fraction after extraction is of high importance as a source of green carbon that could be utilized in metallurgical industries.

Ferroalloys are defined as iron-rich alloys which contain high proportions of Si, Mn, C, Cr [8]. Ferroalloys are produced in submerged-arc furnaces at temperatures $> 1500°C$. Within the furnace, a three-phase electrode is inserted into a mixture consisting of metal oxide and carbonaceous reductants, typically metallurgical coke and coal [9]. The most important properties of the carbonaceous reductant are high reactivity, high conversion and low levels of impurities (such as sulphur and phosphorus) [10]. Low ash content in carbonaceous reductants is an important property because each additional percent of ash can increase slag volume by about 10-15 $kg\ t^{-1}$ of ferroalloy, thereby increasing the electric power required for smelting [11]. Charcoal has low ash content and thus, shows a potential to produce a value-added feedstock for hydrogen storage, electrochemical energy storage with lithium-ion batteries or supercapacitors, activated carbon filtering, gasification and metallurgical industries [12, 13]. The high reactivity of charcoal reductant may be advantageous in some cases within the ferroalloy industries. However, the use of a reductant more reactive than metallurgical coke may increase maintenance costs due to the decreased electrical conductivity [14, 15]. Therefore, reductant reactivity becomes a key variable that must be understood in potential replacements for metallurgical coke. The graphitic or turbostratic structure of charcoal decreases the reactivity and improves the dielectric

properties of solid residues [12, 16]. CO_2 charcoal reactivities were shown to depend mainly on heat treatment temperature, and less on the ash composition of the original feedstocks and residence time. In addition, the reactivities of charcoal from high temperature pyrolysis (2400-2800°C) are similar to those of metallurgical coke emphasizing the importance of graphitizing temperatures on the charcoal behavior [17]. Thus, the influence of pyrolysis operating conditions which affect the charcoal structure and properties will be examined in the present study.

In the forestry sector, utilizing supercritical extraction process has been shown to improve the off-gassing of wood pellets, thus reducing the potential for uncontrolled auto-oxidation, while maintaining pellet properties [3, 18]. Moreover, supercritical CO_2 extraction can also improve the physicochemical properties of solid char from pyrolysis at high temperatures, leading to greater electric conductivity and low reactivity of charcoal [19]. Supercritical CO_2 extraction increases the bending strength and stiffness of residual wood and, thus, decreases the cost of process scaling up, wood storage and transportation [20]. Little is known about the effect that $scCO_2$ extraction has on the various physicochemical properties (elemental composition, density, porosity and dielectric losses) of different wood fractions in terms of the yields and characteristics of pyrolysis products used as charcoal reductants in metallurgical industries. Several methods exist for the extraction of high-value molecules from biomass including conventional organic solvent extraction, hydrodistillation, low-pressure solvent extraction and hydrothermal feedstock processing [21–23]. Supercritical fluids demonstrate properties between those of a liquid and a gas, with the viscosity of a supercritical fluid

being an order of magnitude lower than a liquid, whereas the diffusivity is an order of magnitude higher and thus, leading to the enhanced heat and mass transfer [24]. The properties of a solvent can be fine-tuned by varying the temperature and pressure. Conventional solvents traditionally utilized in wax extraction (such as hexane) are frequently viewed as being problematic due to the toxicological and environmental impacts [25]. Supercritical fluid extraction using CO_2 as a solvent has an easily accessible critical point, is non-flammable, has minimal toxicity and is widely available [26]. Supercritical CO_2 extraction ($scCO_2$) has been conducted on a commercial scale for over two decades for the extraction of high-value products from biomass [27]. Thus, the proposed biorefinery concepts [28–30], which combine the $scCO_2$ extraction and pyrolysis processes, for the exploitation of waste or low value forestry residues for the cost-efficient production of charcoal reductants in ferroalloy industries will be investigated in the present work. As carbonaceous reductants such as charcoal from biomass are potentially more sustainable feedstocks for the ferroalloy industries, the production of this product will be a major focus of this current work.

Utilization of forest residues is constrained and frequently prevented by economic, technical and ecological challenges, which are related to anisotropic properties of wood [31]. The physical and chemical properties of lignocellulosic materials depend on structural (e.g. knots and grain deviation) and environmental (e.g. moisture and temperature) interactions during tree growth [32]. The mineral content and distribution of lignocellulosic compounds show significant variations between tree part (root, stem and branch) [33]. Needles are rich in lipophilic extractives, especially in waxes [34, 35]. Spruce needles

have high phosphorus, sulfur, potassium and calcium contents, whereas the spruce bark contains high amounts of calcium and magnesium [36, 37]. The ash and extractives contents are higher in bark compared to stemwood [38], branch and root wood samples contain more minerals, galactan, xylan and lignin compared to glucomannan rich stemwood [31]. The physical properties such as moisture content, shrinkage, density and permeability are affected by the chemical composition of wood. Importantly, this work aims to investigate the influence of supercritical extraction pretreatment of wood wastes and low value wood residues on the resulting charcoal and tar formation during pyrolysis. Herein, detailed analysis of wood fractions (bark, stem, needles, branches) has been undertaken to understanding the properties of these feedstocks in order to: (1) optimizing solvent extraction processes leading to maximal yields of extractives and (2) optimizing the charcoal production in metallurgical properties. Integrating processes can be important for the development of holistic biorefinery that not only produce fuels such as charcoal, but lead to the generation of bio-based chemicals that may add value to a process. It is envisaged that the charcoal produced through a combination of $scCO_2$ pre-treatment and pyrolysis may provide a cost-efficient charcoal reductant for the metallurgical industries, whilst the pretreatment by scCO2 can yield value added by-products for further application in chemical industries. Extracts from pretreatment have been characterized, the benefits of employing an integrated process are discussed and potential applications for the resulting chemicals will be highlighted. To the author's knowledge, no previous work has been carried out on the characterization of charcoal for the use in ferroalloy industries using $scCO_2$ pre-treatment of biomass. This

work aims to demonstrate the potential benefits of combining technologies for enhancing thermal processes and leading to a greater range of chemical products as part of an integrated holistic biorefinery for fuel and chemical production from wastes.

2. Materials and methods

2.1. Original biomass

Scots pine trees, with an average age of 147 years, were harvested from a forest stand in northern Sweden. Fractions from harvested trees were green needles, branches without needles, and bark from the basal log with a mean cross-sectional diameter of 210 mm. Prior to feedstock characterization, wood fractions were comminuted on a hammer mill (MAFA EU-4B manufacturer, Sweden) with an operating speed of 60 Hz sieved to particle size fractions of 0.05-0.2 mm. Fuel selection in this study was based on the differences in the ash composition and plant cell compounds (cellulose, hemicellulose, lignin, extractives). The compositional analysis of biomass (cellulose, hemicellulose, acid-soluble lignin, acid-insoluble lignin, protein and extractives) was conducted according to NREL technical reports [39–41] and Thammasouk et al. [42].

2.2. Supercritical CO_2 extraction

The $scCO_2$ extractions were conducted using a supercritical extractor SFE 500 (Thar technologies, USA). Supercritical fluid grade carbon dioxide (99.99 %, dip-tube liquefied CO_2 cylinder obtained from BOC) was used in the extractions. The CO_2 supplied from a cylinder as a liquid was maintained

in this state through a cooling unit (-2°C) to avoid cavitation in the high pressure pump, as shown in Figure 1.

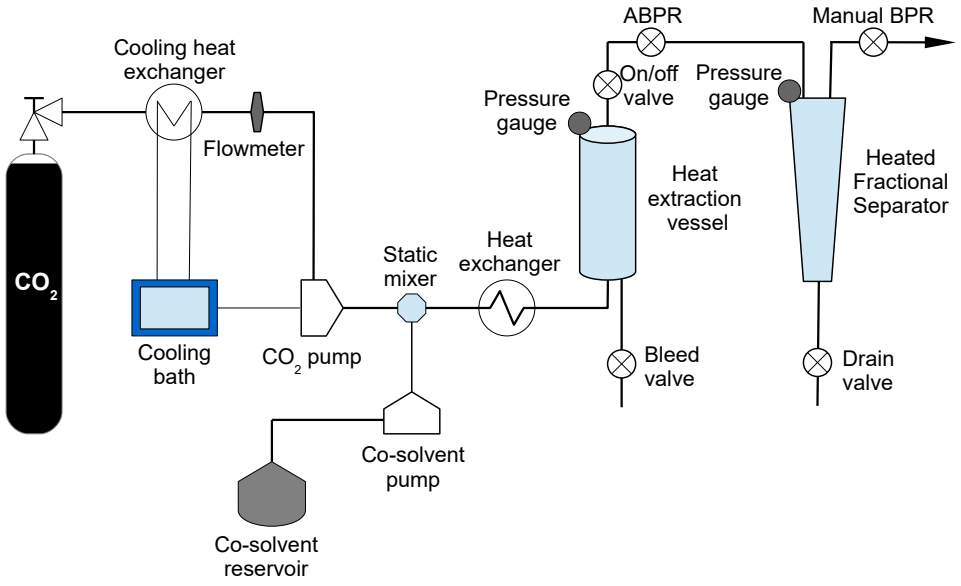

Figure 1: $ScCO_2$ extraction of wood fractions schematic.

The $scCO_2$ extractions of the different biomass types were optimized using a two-level factorial design [18]. Evaluation was made by determination of the extracts' weight in the different experiments. Approximately 180 g of biomass was placed into the 500 mL extraction vessel. The reaction vessel was heated to the required temperature and was equilibrated for 5 min. An internal pump was used in order to obtain the required pressure. The system was run in dynamic mode, in which the carbon dioxide containing the extractives was flowed into the collection vessel. A flow rate of 40 g min^{-1} of liquid CO_2 was applied and the extraction was carried out for 2 h. On completion the system was depressurized over a period of 60 min. Eight ex-

tractions were carried out at various pressures (200, 300 and 400 bar) and temperatures (40, 50 and 60°C). Extractives from supercritical extraction were collected in a fractional separator, samples were then stored in a fridge at 4°C prior to analysis. For a more detailed description of the optimization of the $scCO_2$ extraction process (experimental design etc.) for the different biomass fractions, please see the supplementary materials (Session S-11).

2.3. Slow pyrolysis reactor

The charcoal samples were generated in the slow pyrolysis reactor, as shown in Figure 2. The reactor can be operated at temperatures up to 1350°C and heating rates up to 20°C min^{-1}. The pyrolysis setup encloses a two-stage cooling system with a condensation collector and a pyrolysis gas sampling unit. The pyrolysis retort (inner diameter: 75 mm, height: 150 mm, wall thickness: 2 mm) is made of SiC material. The volume flow of the N_2 gas was measured by the flowmeter HFC-202 (Teledyne, USA). The reactor was continuously purged with nitrogen at a constant flow rate of 100 ml min^{-1}. The temperature control system was based on the LabView software (Version 8.6). The sample mass of 20 g for each experiment was selected. The wood sample was distributed homogeneously in the reactor's retort, pre-heated in nitrogen at 10°C min^{-1} up to 160°C and kept at that temperature for 30 min. The dried wood was further heated at 10°C min^{-1} up to 900, 1000, and 1100°C and kept at the final temperature for about 1 h to ensure complete conversion. After the heating program was finished, the furnace was switched off and the charcoal sample was cooled overnight in N_2 (0.3 l min^{-1}). Samples were stored in sealed plastic containers.

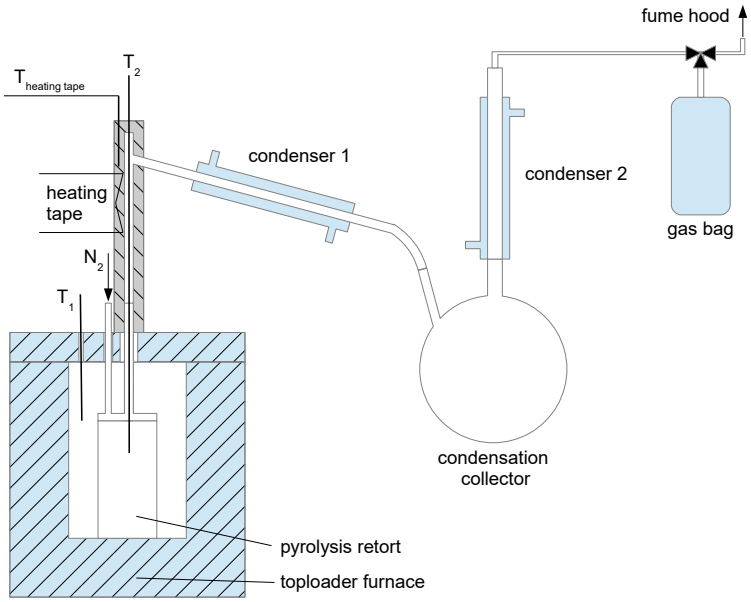

Figure 2: Slow pyrolysis reactor setup.

Under properly selected treatment conditions (e.g. $> 900°C$), charcoal can be produced from renewable sources with low reactivity, high electrical conductivity and low alkali metal content approaching properties of fossil-based metallurgical coke [12, 16, 17, 43, 44].

2.4. Original biomass and charcoal analysis

Elemental analysis. The elemental analysis was performed on an Analyser Series II (Perkin Elmer, USA), according to the procedure described in ASTM D5373-02. Acetanilide was used as a reference standard. The oxygen content was calculated by difference.

Proximate analysis. The proximate analysis was conducted to determine the contents of moisture, ash, volatiles, and fixed carbon according to the pro-

cedures described in ASTM D2216-19, ASTM D1102-84, ASTM D3175-11, and ASTM D3172-13. The high heating value was determined by the bomb calorimeter (IKA C-200) according to the procedure described in ASTM D2015-95.

Ash compositional analysis. The ash compositional analysis was performed by ICP-OES in ASTM D6349-13. Prior to the analysis, biomass samples were pre-heated in oxygen at 10°C min^{-1} up to 550°C and kept at that temperature for 7 h.

Measurement uncertainty. The average standard measurement error in the present study was ±5 wt. %, within a 90 % confidence interval for the proximate, ultimate, ash and lignocellulosic compositional analysis, according to procedures described in ASTM standards [45–50] and NREL technical reports [39–42]. The inaccuracy of biomass analysis was mainly caused by the feedstock heterogeneity and instrument malfunctions [51].

X-ray microtomography. The full 3D microstructure of the wood samples was scanned using x-ray microtomography (XMT, μCT) [52–54], and characterized quantitatively using 3D image analysis. Wood particles, of approximate mass 10 g, were placed in a Kapton tube and scanned using the XMT instrument Zeiss Xradia 510 Versa (Carl Zeiss X-ray Microscopy, Pleasanton, CA, USA). No compression was used in order to prevent any artificial modification of the wood particles [55]. The field of view was 3.96 x 3.96 mm^2 and the spatial resolution in terms of voxel size was 1.96 μm. The x-ray tube voltage and tube power was 50 kV and 4 W, respectively. 3201 projections (radiographs) were collected, with exposure time 2.5 s, over a sample

rotation of 360°, resulting in a total scan time of 5 h. The reconstructed wood structure corresponds to a cylindrical region of diameter 3.8 mm (top), 3.6 mm (bottom) and height 3.96 mm, as shown in Figure 3. 3D quantitative analysis of each wood sample was carried out in three subregions of similar shape, spacial scale and with geometrical location described in Figure 3. The size of each subregion, denoted Part 1-3, was 2.35 x 2.35 x 1.17 mm^3 (1200 x 1200 x 600 voxels). The segmentation was carried out by thresholding, using Otsu's method [56], and quantities such as porosity, number of particles, and volume-to-area ratio were calculated [53, 54]. The porosity was studied on both a global scale (entire ROI), as well as on a particle scale. The particle porosity was calculated as the original binary mask (after segmentation) divided with the corresponding data where all the grains are filled, using a morphologic closing procedure, as described in the supplemental material (Figures S-11-15).

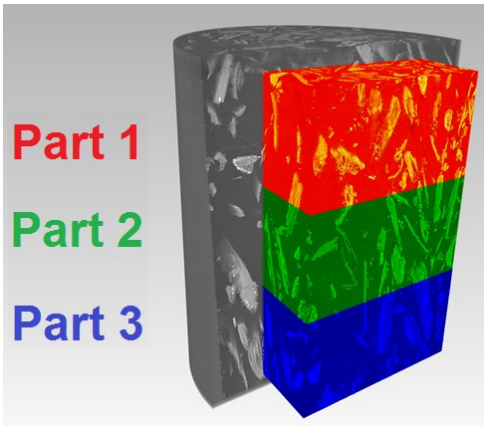

Figure 3: The 3D reconstructed wood samples scanned by x-ray microtomography, were each divided into three subsection, denoted Part 1-3, in which the quantitative analysis of the microstructure was carried out.

Moreover, the volume-to-surface area ratio (V/S) is the total evaluated volume divided by the sum of surface areas from all particles in a volume. The 3D quantitative image analysis and visualizations were carried out using Dragonfly Pro 2.0 software (Object Research Systems, Canada). Additional 2D analysis was carried out for comparison using MatLab R2017a software (MathWorks Inc., USA), and the image processing toolbox.

Mercury intrusion porosimetry. The pore size distribution and porosity of biomass samples were determined by a Pascal mercury intrusion porosimeter system equipped with two instruments. Porosity in the ultramacro and macropore regions was measured by Pascal 140 porosimeter (Micromeritics, Germany) at the low pressures (up to 400 kPa). The Pascal 440 porosimeter equipped with a dilatometer (Micromeritics, Germany) was used to determine the pore size from 1.8 to 7500 nm at high pressures up to 400 MPa. To access the pores and voids within biomass particles, the samples were degassed at room temperature prior to the measurement. Prior to the porosity analysis, wood fractions were dried at 50°C in an oven desiccator for 48 h. The porosity determined with mercury intrusion porosimetry only includes the percentage of open pores that are mercury accessible [57]. The pore sizes in the wood were distinguished into three categories: micropores (1.8-80 nm), mesopores (80-500 nm) and macropores (0.5-58 μm) [57, 58]. The definitions of porosity can be found in the literature [12].

2D dynamic imaging analysis. The particle size and shape of the original biomass were measured using the CAMSIZER XT (Retsch Technology, Germany). The particle size distribution, based on the volume, is represented

by the $x_{Ma,min}$ diameter. For the particle size analysis, ca. 100 mg of sample was used. All measurements were conducted in triplicate to establish sufficient reproducibility within $< 0.5\,\%$. The Martin minimal ($x_{Ma,min}$) and Feret maximal ($x_{Fe,max}$) diameters are suitable parameters to represent the biomass particle width and length in combustion [59]. The particle shape is characterized by sphericity/circularity (SPHT) and aspect ratio (b l^{-1}) in the present study [60].

Karl Fischer titration. Karl Fischer titration was carried out using a KF1000 volumetric titrator (Hach, Germany). Tar samples were first dissolved in anhydrous methanol and then injected into the titration cell. All titrations were carried out at room temperature and the experiments had an error of $\pm$ 0.5 % water content.

Tar analysis. Tar was condensed in two impinger bottles at T = -50°C. Each washing bottle contained 50 mL of methanol because of its good separation from benzene in the DB-EUPAH column in gas chromatography (GC) analyses. The collection efficiency was similar to commonly used isopropanol [61–63]. For the semiquantification of annotated substances, 5 μl of an internal standard (Chlorobenzene, Sigma-Aldrich) was injected in the whole volume of tars dissolved in methanol. Prior to the GC-FID analysis, a 1.5 ml aliquot was pipetted into the autosampler screw cap vial and stored in the freezer at -20°C. The quantitative analysis of tar compounds was performed on a gas chromatograph 7820A (Agilent Technologies, USA) equipped with a flame ionization detector (GC-FID) and DB-EUPAH capillary column (30 m length, 0.25 mm internal diameter, 0.25 μm film thickness). The tempera-

tures of the injector and detector were kept at 250°C and 300°C, respectively. The column temperature program ran from 50 to 280°C. After holding the oven temperature at 50°C for the first 2 min, the temperature was increased to 160°C at a rate of 1.5°C min^{-1}, then to 230°C at a rate of 6°C min^{-1}, and then to 280°C at a heating rate of 8°C min^{-1}; it was then held at this temperature for another 5 min. Nitrogen was used as a carrier gas with a constant flow rate of 1 ml min^{-1}. Data acquisition and processing were performed using Agilent OpenLAB CDS EZChrom A.02.02 (Agilent Technologies, USA). Certain species were calibrated at four levels with solutions of known concentration and 5 replicates per level. Prior to the quantitative analyses in GC-FID, the tar compounds were annotated using a dual detector system GC-MS 5975C TAD Series / GC-FID 7890A (Agilent Technologies, USA). The column temperature and carrier gas settings were kept the same as those used in GC-FID analysis. The mass spectrometer with a quadrapolar type analyzer scanned the range from m/z 35 to m/z 250 resulting in a scan rate of 6.22 scans s^{-1}. The mass spectrometer was operated at unit mass resolution. A 0.5 μl of sample was injected at a 4:1 split ratio. The collected spectra were exported from Chemstation E.02.00.493 (Agilent Technologies, USA) to NetCDF and further processed by the statistical software "R" 2.15.2 [64] that can acquire and align the data, correct baseline, set time-window and perform multivariate analysis [65]. The multivariate analysis using MCR-AR algorithm yielded deconvoluted mass spectra with the well-resolved overlapping peaks [66], which were imported into the mass spectra library software NIST MS Search 2.0 [67]. The area of peaks was normalized to 100 % within each sample and the mean of triplicate measurements was calculated. The

peaks with mass spectra similarity higher than 80 % were used in the tar quantification.

Thermogravimetric analysis. The charcoal samples were firstly crushed to a fine powder in a mortar with a ceramic pestle. The thermal decomposition of charcoal samples was determined using an atmospheric thermogravimetric instrument (Mettler Toledo, USA). The reactivity of charcoal in 20 % volume fraction CO_2 (20 cm^3 min^{-1} of CO_2 and 80 cm^3 min^{-1} of N_2 measured at 20°C and 101.3 kPa) was determined by loading 5 mg of sample in an Al_2O_3 crucible. The charcoal samples were firstly heated up to 110°C and kept for 30 min isothermally for drying. The dried samples were subsequently heated to 1100°C at a constant heating rate of 10 °C min^{-1}. All measurements were conducted in duplicate to establish sufficient reproducibility.

Dielectric measurements. A microwave network vector analyzer N5231A PNA-L (Keysight, USA) was used to measure the dielectric properties of original biomass and charcoal samples at room temperature. To avoid air gaps induced errors during measurements and to obtain comparative results, all samples were grinded, pressed to the same thickness before they were placed in a sample holder. Each measurement was repeated at least three times to ensure accuracy. The dielectric measurements were made with a high-temperature dielectric probe (Agilent 85070) connected via a coaxial cable to the network analyzer. The complex permittivity was measured in the frequency range between 1 and 5 GHz at room temperature. The permittivity (ε) and the loss tangent (tan δ) of the sample are given as [68]:

$$\varepsilon = \varepsilon' - i\varepsilon" \tag{1}$$

$$tan\ \delta = \frac{\varepsilon''}{\varepsilon'} \quad (2)$$

Where ε' is the real part and represents the ability of the dielectrics to store the microwave electrical energy, and ε" is the imaginary part and represents the loss of microwave electrical energy in dielectrics. The loss tangent, which is their ratio, measures the magnitude of the microwave electric field loss in the process.

3. Results and Discussion

3.1. Biomass characterization

The proximate and ultimate analysis of non-treated wood fractions and wood samples after $scCO_2$ extraction is shown in Table 1. The ash compositional analysis was determined for the non-treated Scots pinewood fractions. In supplementary Table S-1, the ash content of non-treated bark and bark after $scCO_2$ extraction remains unchanged, and thus, no differences in the ash composition are expected in other wood fractions.

Table 1: Proximate, ultimate and ash analyses of non-treated Scots pinewood fractions and $scCO_2$ extracted biomass.

Fuel	**Needles**		**Bark**		**Branches**	
	non-treated	$scCO_2$ extracted	non-treated	$scCO_2$ extracted	non-treated	$scCO_2$ extracted
Proximate and ultimate analysis (% on dry basis)						
Moisture[a]	2.5±0.01	2.7±0.02	2.3±0.03	3.1±0.02	0.9±0.02	1.1±0.05
Ash (550 °C)	2.2±0.02	2.3±0.02	0.6±0.04	0.5±0.01	0.8±0.02	1±0.04
Volatiles	80.8±0.05	78.8±0.07	71.6±0.03	70.9±0.06	80.6±0.05	70.9±0.04
HHV[b]	22.4±0.04	21.3±0.04	21.8±0.05	21.3±0.01	21.7±0.02	20.9±0.01
C	53.7±0.07	51.8±0.05	54.7±0.06	54.5±0.08	53.5±0.05	51.4±0.08
H	6.5±0.03	6.3±0.02	5.5±0.04	5.4±0.02	6.2±0.05	5.9±0.01
O	36.1±0.07	38.2±0.05	38.8±0.06	39.4±0.08	39.0±0.05	41.2±0.08
N	1.3±0.01	1.4±0.02	0.3±0.02	0.2±0.01	0.4±0.02	0.5±0.02
S	0.1±0.01	0.1±0.01	0.02±0.002	0.02±0.001	0.03±0.001	0.04±0.002
Ash compositional analysis (mg kg^{-1} on dry basis)						
Cl	0.02±0.001		< 0.01±0.001		< 0.01±0.001	
Al	250±50		250±25		150±60	
Ca	2450±400		1200±100		1300±200	
Fe	70±20		60±20		60±10	
K	5600±500		800±250		2000±200	
Mg	750±80		200±50		400±80	
Na	25±5		10±10		<10±10	
P	1500±100		150±50		400±50	
Si	400±50		350±25		400±70	
Ti	4±4		2±2		6±6	

[a] wt. % (as received) [b] in MJ kg^{-1}

The compositional analysis of wood fractions (cellulose, hemicellulose, acid-soluble lignin, acid-insoluble lignin, protein and extractives) is shown in Table 2.

Table 2: Composition of non-treated Scots pinewood fractions and extractives yield after $scCO_2$ extraction, calculated in percentage based on dry basis (wt. %).

Biomass	**Cellulose**	**Hemi-cellulose**	**Lignin**		**Extractives (raw wood)**	**Extractives (after $scCO_2$ extraction)**
			acid insoluble	**acid soluble**		
Needles	23.4±0.2	15.1±0.1	26.5±0.2	0.5±0.02	12.1±0.02	7.9±0.02
Bark	19.5±0.1	15.1±0.2	45.9±0.3	0.5±0.2	3.9±0.2	2.0±0.1
Branches	25.3±0.2	19.4±0.2	28.0±0.1	1.0±0.2	8.0±0.2	4.4±0.1

3.1.1. X-ray microtomography

Figure 4 shows the 3D cross-sectional slices obtained from XμCT measurements for non-treated pinewood needles and needle fraction after $scCO_2$ extraction. The spacial resolution of 1.96μm is sufficient for observing most features of the needles fibrous network and yielding physically reasonable structural assessments. The characteristic features of milled wood particles such as tracheids, vessels, and pits are observed for both non-treated and $scCO_2$ extracted samples. Figure 4(a) shows the higher level of voids in the non-treated needles than in the $scCO_2$ extracted wood fraction. The segmented tomography images of both pinewood needles in the Supplementary material (Figure S-15) show a wide particle size distribution from 0.01 mm to 12 mm. The XμCT images indicate that the milled pinewood needles are elongated and cylindrically shaped. The width to length ratio increases with the larger particle size of pinewood needles, confirming previous results of Trubetskaya et al. [59]. As seen in the supplemental material (Figure S-12), the global porosity of non-treated and $scCO_2$ extracted pinewood needles is

similar. Thus, the bulk density of non-treated needles ($0.3\,\mathrm{g\ cm^{-3}}$) is only slightly higher than that of the $scCO_2$ extracted needles ($0.29\,\mathrm{g\ cm^{-3}}$).

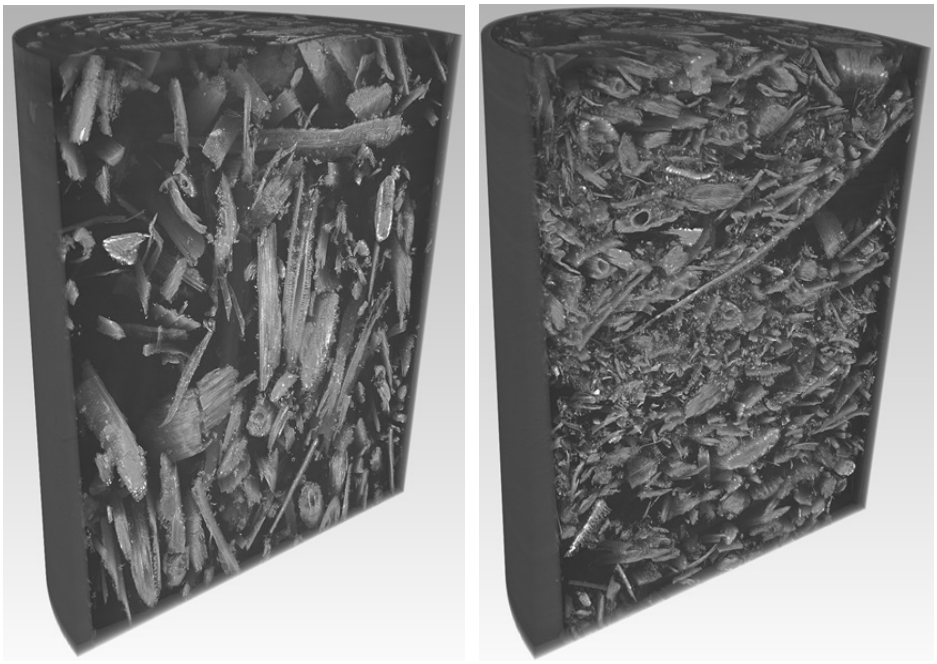

4(a): Non-treated needles 4(b): Needles after $scCO_2$ extraction

Figure 4: XμCT imaging analysis of non-treated needles and $scCO_2$ extracted needles.

Moreover, the bulk density determined using the global porosity from the XμCT analysis is comparable with the value determined for both samples using the pycnometer method as shown in Figure 5(a). The non-treated pinewood needles exhibited a lower porosity than the $scCO_2$ extracted wood particles, confirming the results in section 3.1.3. $scCO_2$ extraction increases the accessibility of wood fractions due to the structure collapse or further lignocellulosic compound redistribution, leading to the increased porosity [69,

70]. However, the porosity of needles determined by XμCT was on average 45 % lower than the porosity measured by the mercury intrusion porosimeter and calculated by skeletal density. This is because the mercury intrusion porosimeter measures pores down to 3 nm compared to the 1.96 μm resolution of XμCT instrument, as reported by Weber et al. [71]. The volume-to-surface area ratio were calculated using the 3D data from XμCT for both non-treated and $scCO_2$ extracted needles. The results showed that the volume-to-surface area ratio, determined using the 2D dynamic imaging analysis (non-treated needles: 0.0037 mm; extracted needles: 0.0056 mm), was lower than the ratio calculated from XμCT data (non-treated needles: 0.003 mm; extracted needles: 0.0057 mm). In the 2D dynamic imaging, a particle is represented as an ellipsoid with the thickness assumed to be equal to the width. The previous microscopy results showed that the particle thickness of woody and herbaceous feedstocks can be estimated to be 1/2 of the particle width [59]. In 2D dynamic imaging, the shape of irregular biomass particles is commonly quantified by using equivalent shape models (i.e. a sphere, an ellipsoid, a cuboid), leading to the underestimation of the real particle surface area [72]. Three-dimensional image analysis using the XμCT enables the characterization of the true physical size of irregular biomass particles based on the results of Hamdi et al. [73].

3.1.2. Biomass density

The bulk densities of non-treated bark, needles, and branches and samples after $scCO_2$ extraction are shown in Figure 5(a). The bulk density of non-treated wood fractions is in the range of 0.25-0.34 g cm^{-3}. The $scCO_2$ extraction of wood fractions does not affect the bulk density significantly,

except for the increased bulk density of bark. The results show overall the bulk density decrease with increasing particle length.

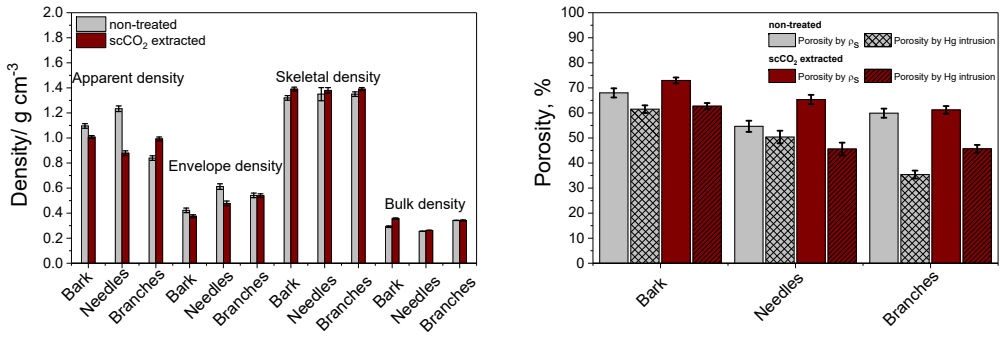

5(a): Densities

5(b): Porosity

Figure 5: Bulk, skeletal, envelope, and apparent density and porosity by skeleton density and Hg intrusion of non-treated bark, needles, and branches and $scCO_2$ extracted wood fractions.

The skeletal density of wood fractions is in the range of $1.4\,\mathrm{g\ cm^{-3}}$, that increased slightly after $scCO_2$ extraction. Brewer et al. [74] reported that the envelope density varies substantially with feedstock due to the differences in cell shape and size distribution. Thus, the porosity of biomass fractions might be affected by the removal of extractives leading to the lower density. The apparent density of bark and needles decreases during the $scCO_2$ extraction. This could be due to the increased micropore content [69]. Figure 5(b) demonstrates large differences in porosities determined by skeletal density and mercury intrusion for the non-treated wood fractions and $scCO_2$ extracted samples. For the non-porous samples, the skeleton and apparent densities are equal. The large differences in porosity determined by skeletal density and mercury intrusion might be attributed to the presence of microp-

ores in the wood fractions. In addition, the variations in plant cell wall composition (cellulose, hemicellulose, lignin, extractives) and the pore geometry might lead to the differences in porosity among the wood fractions [75, 76].

3.1.3. Pore size and porosity

Table 3 shows that untreated needles, bark, branches and samples after $scCO_2$ extraction possess a high ratio of macropores in the range of 90-96 % owing to the occurrence of tracheids, with diameters ranging from 18 to 54 μm for earlywood and from 12 to 25 μm for latewood [77].

Table 3: Pore size and pore size distributions of non-treated bark, needles, and branches and samples after $scCO_2$ extraction characterized by mercury intrusion porosimeter.

Fuel	**Bark**		**Needles**		**Branches**	
	Non-treated	$scCO_2$ extracted	Non-treated	$scCO_2$ extracted	Non-treated	$scCO_2$ extracted
Macropores, %	90±0.1	96±0.2	97±0.2	95.3±0.1	93±0.1	94.7±0.2
Mesopores, %	7±0.05	3.8±0.04	3±0.02	3.3±0.02	5±0.01	3.7±0.03
Micropores, %	3±0.02	0.1±0.01	2±0.02	1.4±0.03	2±0.02	1.6±0.01
V_{cum}, $mm^3\ g^{-1}$	1520±0.3	1840±0.2	900±0.4	1040±0.2	676±0.2	940±0.1
SSA, $m^2\ g^{-1}$	7±0.01	3.6±0.02	0.7±0.01	1.8±0.02	5.3±0.02	9.3±0.02
Average pore diameter, μm	0.9±0.01	2±0.02	5±0.02	2.3±0.01	0.5±0.005	0.4±0.004
Median pore diameter, μm	20±0.02	26±0.03	43±0.06	30±0.02	8.6±0.01	20±0.01

The amount of micropores and mesopores in wood fractions is low, corresponding to results of Reyes et al. [69]. This could be accounted for by the submicroscopic pore system within the cell wall, small apertures within the resin canals and pits [78, 79]. The range of mesopores complies with the apertures of the pits which have an average diameter of 200 nm and continuous canals within the epithelium tissue [80]. The average pore size

of the high lignin containing bark and branches varied only slightly during $scCO_2$ extraction. The extraction of needles resulted in a larger percentage of micro- and mesopores, leading to the specific surface area increase. The higher cumulative pore volume of wood fractions after extraction is caused by the high content of micropores with poorer accessibility as reported by Plötze and Niemz [57]. The results indicate that the wood $scCO_2$ extraction affects the pore size and volume only slightly.

3.2. Particle size and shape

The particle size and shape of non-treated wood fractions and samples after $scCO_2$ extraction were analyzed by CAMSIZER XT instrument. The results of the particle characterization study indicate nearly similar particle size of all wood fractions, as shown in the supplemental material (Figure S-3). The particle shape of samples was characterized using the sphericity (SPHT) and width/length ratio (b/l) parameters. The wood fractions obtained cylindrical or rectangular shapes (SPHT = 0.5-0.8; b/l ratios = 0.5-0.7). It seems that the needles are more elongated (b/l $\approx$ 0.5) than other wood fractions. The bark samples showed the smallest changes in particle size and shape in the extraction process. The results of particles > 0.25 mm in terms of shape description were considered as non-representative due to the low presence of particles in this fraction. The effect of $scCO_2$ extraction is overall negligible on the particle size and shape of scots pinewood fractions.

3.3. Extractives yields

Total amounts of extractives are shown in Figure 6.

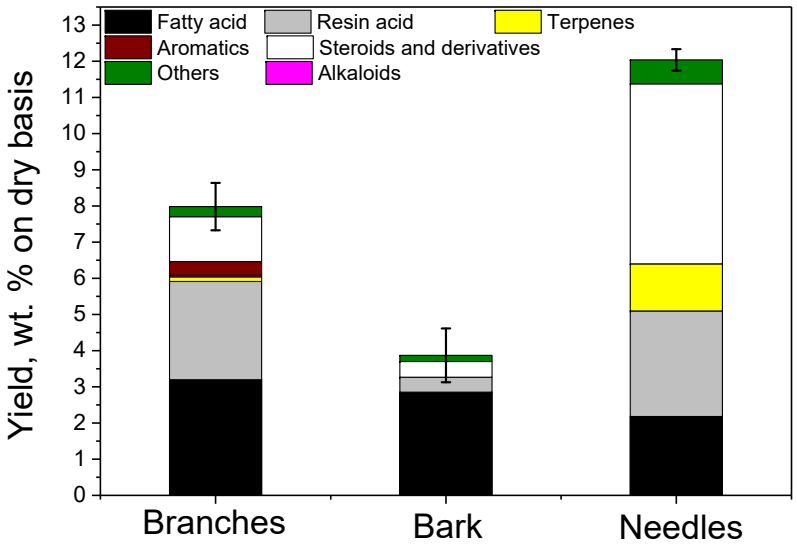

Figure 6: Yields of extractives from $scCO_2$ treatment of needles, bark and branches.

The largest amount of extractives (11 wt.%, db) was determined in needles, whereas the extractives content was significantly lower in branches (about 7 wt.%, db) and bark (about 3.7 wt.%, db). It is well known that the proportion and composition of extractives varies considerably depending on the part of the tree being analyzed [81]. The extraction of needles led to significantly greater yields of steroids and derivatives, terpenes and other extractives than the extraction of branches and bark. Sterols are important for membrane stability, growth and reproduction in plants [82–84]. Significant information is already known about the composition and proportion of tree sterols. Studies have demonstrated that needles contained highest amounts of free sterols, which is a reflection of the increased membrane production at this stage of plant development, while in mature needles the free and es-

terified sterols are in even proportions [85, 86]. In the case of the trunk it is known that the center contains a greater proportion of extractives including free and esterified sterols [87, 88]. These findings are consistent with the lower proportions of extractives including sterols observed in the bark and branches of this current study. The extraction of needles and branches gave similar yields of resin acids which were greater than the yields from the bark extraction.

3.4. Charcoal characterization

3.4.1. Product yields

The mass balances of the slow pyrolysis experiments with respect to measured solid residue (charcoal) and major liquid products (water and organic fraction), dependent on the heat treatment temperature, are shown in Figure 7.

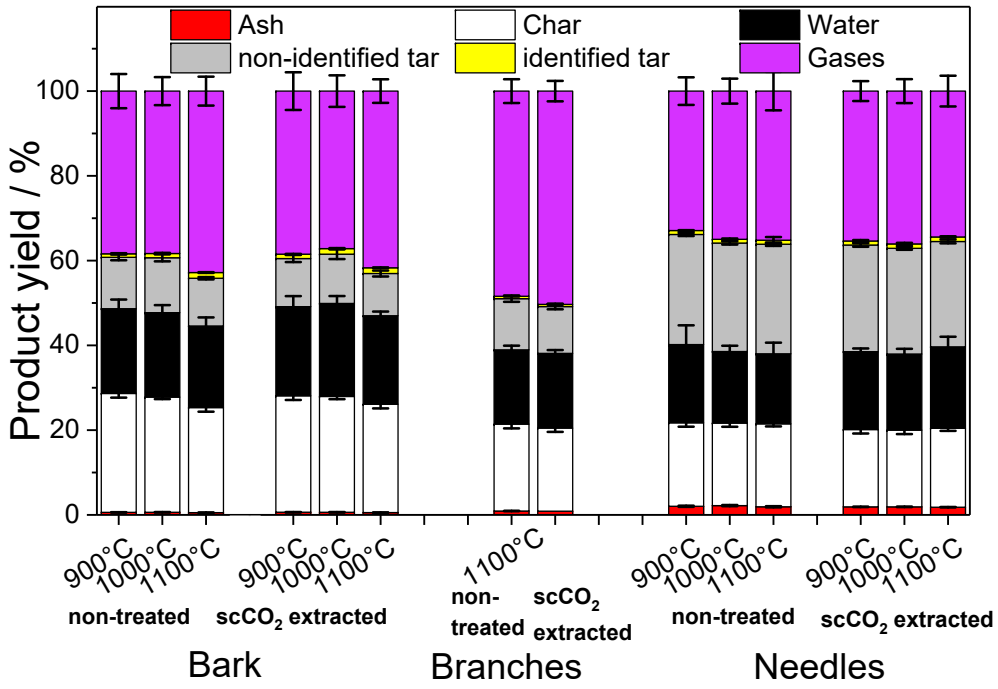

Figure 7: Tar and charcoal yields (wt. % relative to the non-treated biomass) of needles, bark and branches, reacted at 900-1100°C in the slow pyrolysis reactor. The total yield of charcoal is separated in ash and organic matters. The total yield of tar is separated in organic fraction and water content. The error bars characterize the deviations between the total yields of products.

The amount of gaseous species was not measured in the present study, but estimated by the difference from the mass balance. The mass balances represent an average of two measurements. The charcoal yields from pyrolysis of needles, bark and branches were similar at 900, 1000 and 1100°C. The differences in product yields of non-treated wood fractions and samples after $scCO_2$ extraction were small. The charcoal yield from pyrolysis of needles was lower than that from pyrolysis of bark and vice versa with the liquid product

yields due to the higher lignin content and lower amounts of extractives in bark. This observation was confirmed by the similarly lower charcoal yields of branches and needles compared to that of bark. In contrast, the liquid product yields of bark and branches generated at 1100°C were similar due to low content of remaining extractives after $scCO_2$ treatment.

3.4.2. Tar analysis

The identification of individual tar compounds was based on the present results of GC-MS analysis, PAH pattern recognized in the literature and comparison with the reference chromatograms of external standards. The identified tar compounds with the relevant information were listed in the supplemental material (Table S-3). Forty five compounds in the pyrolysis tar have been quantified and grouped for the further modeling using SIMCA, as reported previously [63]. Figure 8 shows the change in the yields of tar from pyrolysis of non-treated needles, branches and bark and fractions after $scCO_2$ extraction in the range from 900 to 1100°C. The pyrolysis of both non-treated and $scCO_2$ extracted bark gave a greater tar yield compared to other wood fractions. The yield of identified tar from non-treated branches was the lowest (5.5 mg g^{-1}-sample), whereas the yield of identified tar from $scCO_2$ extracted bark was the greatest (13.5 mg g^{-1}-sample). In general, the tar yields of non-treated wood fractions were lower than the tar yields from pyrolysis of $scCO_2$ extracted samples. This may also show that the presence of resin or fatty acids in pinewood could decrease tar formation during pyrolysis.

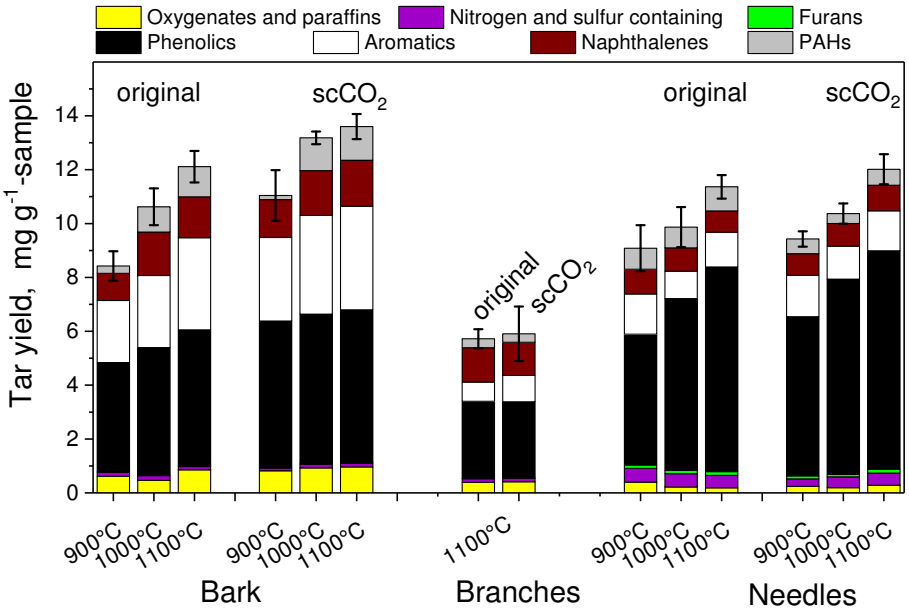

Figure 8: Tar yields (mg g^{-1} on dry basis) of non-treated needles, bark and branches and $scCO_2$ extracted wood fractions.

Moreover, greater yields of aromatic, naphthalenes, oxygenates and paraffins were observed in tar from bark pyrolysis, whereas needles tar obtained greater concentrations of phenolics, furans, nitrogen and sulfur containing compounds compared to tars from pyrolysis of bark and branches. The tar yields increased with the increased heat treatment temperature. In pyrolysis of bark, the tar yields increased due to the greater yields of aromatic compounds, whereas tar yields in pyrolysis of needles increased due to the increase in concentration of naphthalenes.

3.4.3. Thermogravimetric analysis

The CO_2 reactivity of charcoal samples was investigated under CO_2 gasification condition in a thermogravimetric analyzer due to the importance of the reaction between charcoal and carbon dioxide. In ferroalloy industries, the carbon dioxide passes through the burden of charcoal and is further reduced to carbon monoxide according to the highly endothermic Boudouard reaction, as shown in equation 3 [89]:

$$C + CO_2 -> 2CO \tag{3}$$

Figure 9 shows differential weight loss curves (DTG) for the 20 % volume fraction CO_2 gasification of solid residues from pyrolysis. The DTG curves show a single broad peak in CO_2 gasification, indicating a heterogeneous charcoal mixture with respect to the composition and particle size as suggested by Russell et al. [90]. The maximal reaction rates of charcoal samples of non-treated and $scCO_2$ bark and branches were similar at nearly 1065 and 1020°C and less than the maximum reaction rates of non-treated and $scCO_2$ extracted needles. This is probably due to the catalytic effect of alkali metals that increases the CO_2 reactivity of charcoal from pyrolysis of high ash containing needles [91]. The maximum reaction rate of charcoal from pyrolysis of $scCO_2$ extracted needles at 900 and 1000°C was about 100°C greater than that of charcoal from non-treated needles. Moreover, the charcoal of non-treated needles from pyrolysis at 1100°C was slightly less reactive than the charcoal of $scCO_2$ extracted needles.

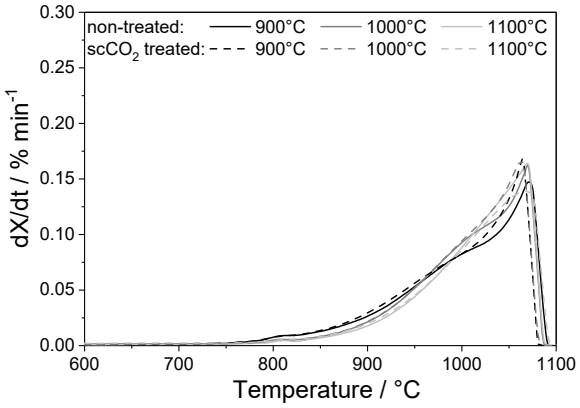

9(a): Bark

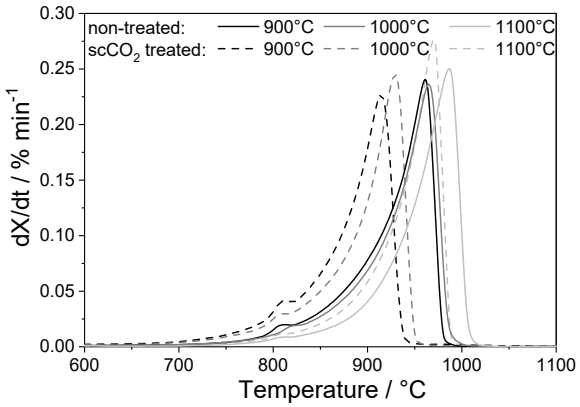

9(b): Needles

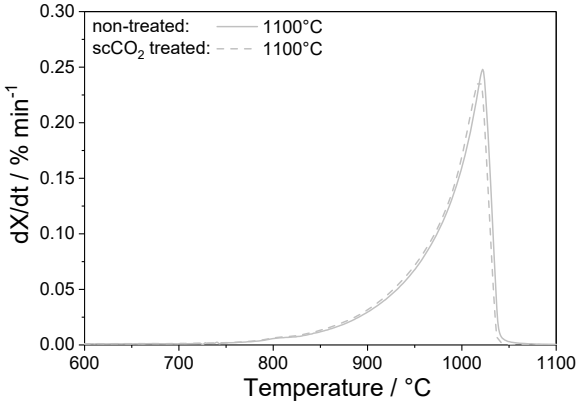

9(c): Branches

Figure 9: DTG curves of charcoal from non-treated wood fractions and $scCO_2$ treated biomass samples pyrolyzed at 900, 1000, and 1100°C in the DTF and further reacted in 20 % volume fraction CO_2 + 80 % volume fraction N_2.

3.4.4. Dielectric measurements

The relative dielectric constant ε' and dielectric loss tangent tan δ of non-treated biomass, $scCO_2$ extracted wood fractions and charcoal samples are shown in Figure 10. The dielectric constant smoothly decreased with frequency. Therefore, the frequency-dependence behavior for all charcoal samples is largely in agreement with that for activated carbon and coal chars [68, 92]. The ε' of charcoal samples increased with the increased heat treatment temperature during pyrolysis. The dielectric properties of prepared charcoal samples were greater compared to all raw biomass samples which could indicate that the carbon structure in these charcoal samples have changed dramatically after pyrolysis. The loss of moisture and oxygen-containing functional groups in biomass skeleton could lead to a greater C/O ratio that increased as the heat treatment temperature increased. The $scCO_2$ extraction of wood led to even higher C/O ratio biomass to start with and hence higher dielectric properties were observed for charcoal samples from $scCO_2$ extracted wood compared to non-treated ones at the same heat treatment temperature. The results also indicate an increase in content and structure ordering of carbon in generated charcoal samples had occurred as the heat treatment temperature increased, as reported by Alias et al. [93]. The heat treatment of biomass enhances the dielectric losses and therefore more heat is generated inside charcoal, indicating that charcoal is a microwave prone material [92]. Figure 10 shows that the tan δ values of charcoal samples range from 0.4 to 1.6 at the maximum frequency and are greater than that of biomass due to the increase in a surface area and carbon content with the heat treatment. Overall, the $scCO_2$ extraction had also an impact on the

dielectric properties of charcoal.

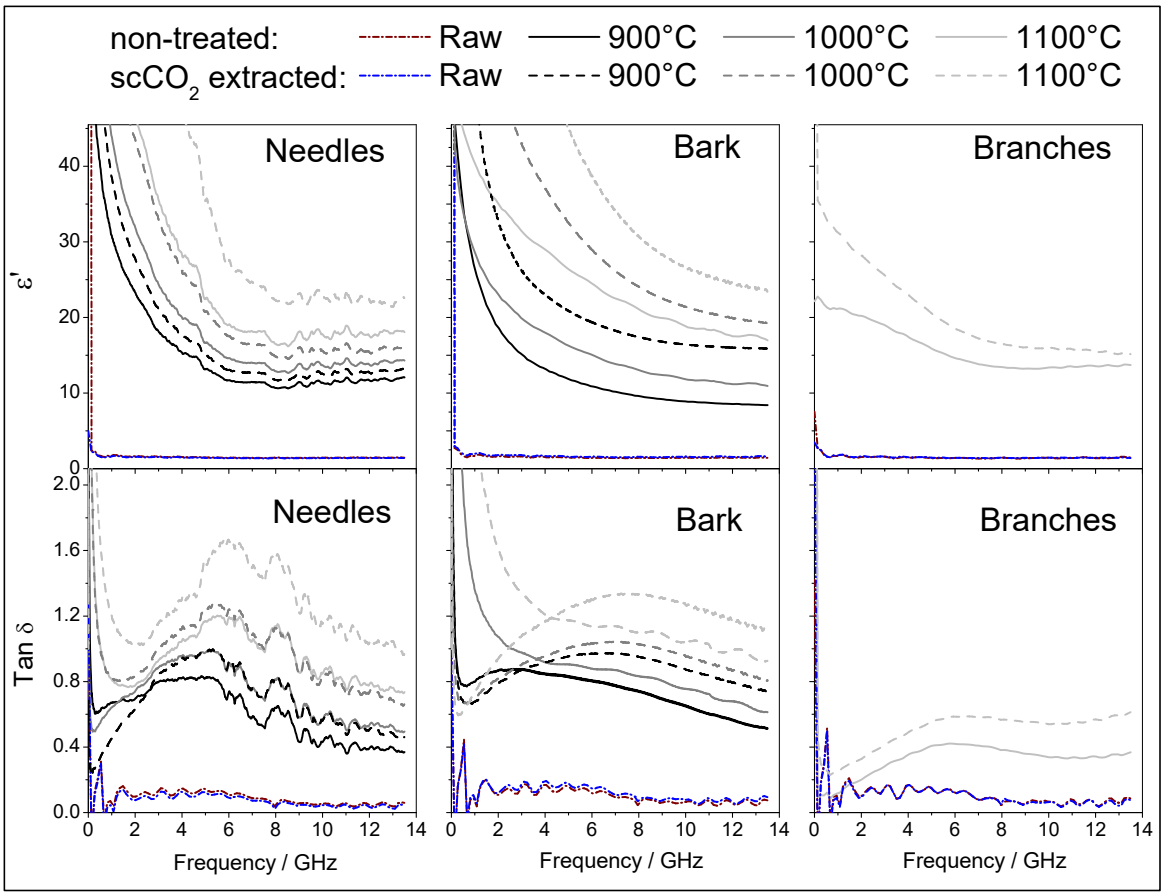

Figure 10: Dielectric constant ε' and dielectric loss tangent tan δ of non-treated biomass, $scCO_2$ treated wood fractions and charcoal samples.

In general, the ε' values of charcoal samples varied from 8 to 25, approaching dielectric properties of activated carbons (20-40) [94]. The increase in heat treatment temperature led to the formation of more ordered carbon in charcoal structure [12]. Breaking of aliphatic hydrocarbon groups and formation of large polyaromatic structures result in stacking of aromatic carbon

rings in charcoal samples [95]. Thus, conduction losses would be experienced in charcoal samples due to the π-electron conjugation within the ordered carbon domains which experience higher dielectric properties. Stronger carbon-carbon π-bonds could be formed between compressed polyaromatic carbon layers at high temperatures, whereas the π-bond localized electron in turbostratic charcoal structure contributes to dielectric permittivity through the high polarization [96, 97]. The results indicate that bark charcoal was more dipolar than needles and branches charcoal samples obtained from pyrolysis at 1100°C. This is due the greater lignin content in original bark compared to other wood fractions, as reported by Ben et al. [98]. The hydroxyl groups are strongly polarized with high hydrophilic properties. The high content of non-polar groups in lignin fibers and polar groups in pinewood bark results in the dipole formation and thus, better dielectric properties of bark charcoal. Moreover, the alkali rich needles and branches could decrease the orientation of polarization in the carbonaceous charcoal matrix and thus, decrease the dielectric constants of needles and branches charcoal samples [99]. The dielectric constants of $scCO_2$ treated charcoal samples were slightly greater than that of charcoal samples from pyrolysis of non-treated biomass. The differences in the dielectric properties of charcoal from non-treated biomass and $scCO_2$ extracted wood fractions were related to the differences either in density of original wood, stacking of aromatic rings in the charcoal, type of oxygen functional group (i.e. OH, CHO, ether, COOH) or moisture content, consistent with the previous results of Ramasamy et al. [100]. The $scCO_2$ extracted wood fractions are more dense than the non-treated pinewood and thus, more polar groups can accompany dielectric polarization, improving

the dielectric properties of non-treated wood and charcoal samples [101]. In comparison with the hydrothermal carbonization and microwave pyrolysis, charcoal produced from wood fractions at high temperatures in slow pyrolysis contains more fixed carbon and less volatile components leading to greater dielectric properties due to the extent of graphitization of charcoal structure [19, 102–104].

3.4.5. Economic assessment of supercritical extraction process and potential applications of extracts

In order to evaluate the viability of the supercritical extraction process, an economic assessment was carried out, based on a model by Turton et al. [105]. This model has been used extensively, especially in supercritical processes, in order to estimate the cost of manufacture (COM) of a chemical product. It has been shown to be effective in estimating the COM of supercritical extraction processes with regards to extraction of waxes, essential oils, resin acids among other components [21, 106–108]. With this model, the COM is calculated in terms of five main costs; fixed capital investment (FCI), cost of operational labour (C_{OL}), cost of raw materials (C_{RM}), cost of utilities (C_{UT}) and cost of waste treatment (C_{WT}):

$$COM = 0.28 \cdot FCI + 2.73 \cdot C_{OL} + 1.23 \cdot (C_{RM} + C_{WT} + C_{UT}) \qquad (4)$$

The detailed techno-economic evaluation is discussed in the supplemental material. Due to limited data available, the FCI is based on a small industrial supercritical extraction unit, that is employed for the extraction of spices, natural pigments, essential oils etc., having an annual capacity of approximately 2000 t y^{-1}. An extensive breakdown and explanation of the costs

and calculations involved may be found in the Economic Sentiment Indicator (ESI). The COM was calculated for each type of biomass in this study, i.e. needles, bark and branches. The COM for the supercritical extraction processes was found to be approximately: (1) € $5.71\,\mathrm{kg}^{-1}$ extract from needles (€ $541.18\,\mathrm{t}^{-1}$ needles) (2) € $8.63\,\mathrm{kg}^{-1}$ extract from branches (€ 429.51 t^{-1} branches) (3) € $20.35\,\mathrm{kg}^{-1}$ extract from bark (€ $448.69\,\mathrm{t}^{-1}$ bark). The difference in COM between the different biomass is attributed to the difference in % yield extract obtained (which has the most significant effect on the COM) - the needles have the highest yield per extraction with a yield (7.9 %) followed by the branches and the bark. Overall, this study has shown that, if certain parameters are taken into account, high value products (waxes, essential oils, resin acids) can be obtained for a low price. Although the value for the bark is quite high, a number of assumptions have been conducted in this study. Firstly, as previously stated, the model was based on a small industrial scale supercritical unit ($2000\,\mathrm{t\ y}^{-1}$) as a result of the limited data available in the literature with regards to supercritical extraction facilities. Literature has shown that, although the initial FCI would increase, scaling up from $2000\,\mathrm{t\ y}^{-1}$ to a $10000\,\mathrm{t\ y}^{-1}$ (or higher) could substantially lower the COM by over half of that reported here - this is as a result of a significantly higher throughput combined with automated handling of material that would reduce COL [109]. Secondly, it is assumed in this model that the COM is solely for the supercritical extraction process. Since the $scCO_2$ extraction of lipids from forestry residues is conducted as part of a biorefinery setup, i.e. the forestry residues post-extraction will be passed on for downstream processing (microwave pyrolysis and gasification) - which would further lower

the COM as things such as CRM will be distributed over the entire process. Finally, some other factors that could be considered are: construction of the supercritical plant at the site of collection in order to reduce costs relating to storage and transport of the biomass.

Although $scCO_2$ extraction is regarded as a high energy process, it can lead to a number of significant benefits when applied as part of an integrated biorefinery that produces both fuels and chemicals. Importantly, supercritical extraction had limited effect on the yield of the resulting charcoal, but had a beneficial effect on the tar yields, leading to an increase in naphthalene, polycyclic aromatic hydrocarbons, aromatic and phenolic fractions with greater temperature, $scCO_2$ extraction also led to the isolation of value added chemicals from the various different forest residues, thus providing a host of platform molecules that can be utilised in a wide range of industrial applications. The recovery of such products would be of benefit in an integrated biorefinery that not only produces fuels but also yields chemicals, and material products too.

The following section highlights the potential applications of the extractives obtained via supercritical extraction of waste wood feedstocks. Extracts from the Scots Pine needles have been found to have considerable quantities of nonacosan-10-ol, a secondary long-chain alcohol. Previous studies have shown that it can be isolated and purified via a simple, efficient, one-step process and this molecule has been shown to show significant promise as a renewable alternative for use in superhydrophobic coatings due to the molecule being highly hydrophobic in nature [110].

There is major promise to utilise the large quantities of resin acids,

present in the different extracts, in phyto-epidemiological and pharmacological applications due to the high bioactivity displayed by these compounds. Resin acids such as isopimaric acid and dehydroabietic acid, which are present in considerable quantities in the extracts, demonstrate significant antifungal and antibacterial activities, while studies have shown abietic acid to have anti-thrombotic and anti-inflammatory properties [111–114]. In fact, abietic acid derivatives have been investigated in drug-delivery applications [115]. In addition, rosin, which constitutes primarily of abietic acid and pimaric acid, is currently utilised in a host of applications including paints, inks, varnishes, cosmetics and in chewing gum [116]. Present in the extracts are also saturated and unsaturated fatty acids (e.g. C_{18} saturated and unsaturated acids), which can be a renewable feedstock for polymer applications and production of lubricants [4]. Fatty acids also find use in the production of detergents, soaps, cleaning products and polishes [5]. The benefits of unsaturated fatty acids as nutraceuticals for lowering levels of cholesterol in the blood have been well documented [6]. Free phytosterols, present in the extracts of the needles, have been shown to demonstrate an array of nutraceutical and pharmaceutical properties, from reducing LDL-cholesterol levels in the blood to demonstrating anticancer activity (in different types of cancers including breast, prostate and colon cancer) [117].

4. Conclusion

Different pinewood fractions were converted into renewable charcoal by pyrolysis treatment. The novelty of this work relies on the fact that the high heat treatment temperatures and high lignin content in biomass improve the

dielectric properties and increase graphitization of charcoal. The pretreatment using $scCO_2$ extraction of wood enables the removal of more than half of value-added compounds without any significant influence on the physical properties of original wood and on the yield of solid charcoal. However, the presence of extractives in original pinewood showed properties which reduce the formation of tar during slow pyrolysis. Under properly selected treatment conditions (e.g. $> 1100°C$), charcoal samples can be produced from a mixture of different low quality wood fractions with reactivity and dielectric properties approaching that of fossil-based metallurgical coke and with the low content of liquid products, including naphthalene, PAHs, aromatic and phenolic fractions. The findings of this study supported by the techno-economic analysis emphasizes the potential use of supercritical extraction as a pretreatment of low value forestry residues in the production of biocarbon-based reductants for application in the ferroalloy industries, with concomitant reductions in CO_2 emissions.

Acknowledgements

The authors gratefully acknowledge financial support from FORMAS (CETEX project), Kempe Foundation, Björn Wahlströms, and Jernkontoret Stiftelsen. The authors acknowledge the facilities and technical support of Gundula Stein from GNF Berlin Adlershof e.V. Dr. Daniel Eriksson from Swedish University of Agricultural Sciences in Umeå is acknowledged for the preparation of pinewood fractions. Andrew Hunt would like to acknowledge the financial support of Thailand Research Fund (RSA6280031) and Khon Kaen University. Financial support from the Center of Excellence for Inno-

vation in Chemistry (PERCH-CIC), Ministry of Higher Education, Science, Research and Innovation is gratefully acknowledged. We are grateful to the plant cell wall and carbohydrate analytical facility at UPSC/SLU, supported by Bio4Energy and TC4F for the GC-MS analysis. The authors acknowledge the facilities and technical support of Dr. Junko Takahashi-Schmidt at Umeå Plant Science Centre.

References

[1] Pardo de Donlebun JPA, The EU enlargement in 2004: analysis of the forestry situation and perspectives in relation to the present EU and Sweden. Skogsstyrelsen National Board of Forestry. Jönköping: Sweden; Report No. ISSN1100-0295 (2003).

[2] de Jong J, Akselsson C, Berglund H, Egnell G, Gerhardt K, Lönnberg L and etc., Consequences of an increased extraction of forest biofuel in Sweden. Swedish Energy Agency. Eskilstuna: Sweden; Report No. ISSN1403-1892 (2014).

[3] Attard TM, Arshadi M, Nilsson C, Budarin VL, Valencia-Reyes E, Clark JH and etc., Impact of supercritical extraction on solid fuel wood pellet properties and off-gassing during storage, Green Chem 18 (2016) 2682–90.

[4] Hill K, Fats and oils as oleochemical raw materials, Eur J Pharm Sci 72 (2000) 1255–64.

[5] Ruston NA, Commercial uses of fatty acids, American Oil Chemists' Society 29 (1952) 495–8.

[6] Gill I, Valivety R, Polyunsaturated fatty acids: 1. Occurrence, biological activities and applications, Trends Biotech 15 (1997) 401–9.

[7] White K, Lorenz N, Potts T, Penney WR, Babcock R, Hardison A and etc., Production of biodiesel fuel from tall oil fatty acids via high temperature methanol reaction, Fuel 90 (2011) 3193–9.

[8] Holappa L, Towards sustainability in ferroalloy production, J South African Inst Min Metal 110 (2010) 1–8.

[9] Liu J, Chen Z, Ma W, Wei K, Ding W, Application of a Waste Carbon Material as the Carbonaceous Reductant During Silicon Production, Silicon (2018) 1–9.

[10] Pistorius PC, Reductant selection in ferro-alloy production: The case for the importance of dissolution in the metal, J South African Inst Min Met 1 (2002) 33–6.

[11] Sahajwalla V, Dubikova M, Khanna R, Reductant characterisation and selection: implications for ferroalloys processing, 10^{th} Int Ferroalloys Congress INFACON X. Transformation through Technology 68 (2004) 351–62.

[12] Surup GR, Heidelmann M, Kofoed Nielsen H, Trubetskaya A, Characterization and reactivity of charcoal from high temperature pyrolysis (800–1600°C), Fuel 235 (2019) 1544–1554.

[13] Riva L, Surup GR, Buø TV, Nielsen HK, A study of densified biochar as carbon source in the silicon and ferrosilicon production, Energy 181 (2019) 985–96.

[14] Yamagishi K, Endo K, Saga J, A comprehensive analysis of the furnace interior for high-carbon ferrochromium, 1^{th} Int Ferroalloys Congress INFACON 74. Transformation through Technology (1974) 143–7.

[15] De Waal A, Barker IJ, Rennie MS, Klopper J, Groeneveld BS, Electrical Factors Affecting the Economic Optimization of Submerged-arc

Furnaces, 6^{th} Int Ferroalloys Congress INFACON 6. Transformation through Technology 1 (1974) 247–52.

[16] Surup GR, Eidem PA, Kofoed Nielsen H, Vehus T, Trubetskaya A, Characterization of renewable reductants and charcoal-based pellets for the use in ferroalloy industries, Energy 167 (2019) 337–45.

[17] Surup GR, Heidelmann M, Schubert D, Deike R, Foppe M, Trubetskaya A and etc., The effect of feedstock origin and temperature on the structure and reactivity of char from pyrolysis at 1300-2800°C, Fuel 235 (2019) 306–16.

[18] Arshadi M, Hunt AJ, Clark JH, Supercritical fluid extraction (SFE) as an effective tool in reducing auto-oxidation of dried pine sawdust for power generation, RSC Adv 2 (2012) 1806–9.

[19] Budarin VL, Shuttleworth PS, Dodson JR, Hunt AJ, Lanigan B, Marriott R and etc., Use of green chemical technologies in an integrated biorefinery, Energy Environ Sci 4 (2011) 471–9.

[20] Smith SM, Sahle Demessie E, Morrell JJ, Levien KL, Spliethoff H, Ng H, Supercritical fluid (SCF) treatment: its effect on bending strength and stiffness of ponderosa pine sapwood, Wood Fiber Sci 25 (1993) 119–23.

[21] Pereira CG, Meireles MAA, Economic analysis of rosemary, fennel and anise essential oils obtained by supercritical fluid extraction, Flav Frag J 22 (2007) 407–13.

[22] Chemat F, Abert Vian M, Cravotto G, Green Extraction of Natural Products: Concept and Principles, Int J Mol Sci 13 (2012) 8615–27.

[23] Ruiz HA, Rodriquez-Jasso RM, Fernandes BD, Vicente AA, Teixeira JA, Hydrothermal processing, as an alternative for upgrading agriculture residues and marine biomass according to the biorefinery concept: A review, Renew Sustain Energy Rev 21 (2013) 35–51.

[24] Hunt AJ, Sin EHK, Marriott R, Clark JH, Generation, Capture, and Utilization of Industrial Carbon Dioxide, ChemSusChem 3 (2010) 306–22.

[25] Sin EHK, Marriott R, Hunt AJ, Clark JH, Identification, quantification and chrastil modelling of wheat straw wax extraction using supercritical carbon dioxide, Comptes Redus Chimie 17 (2014) 293–300.

[26] Brunner G, An Introduction to Fundamentals of Supercritical Fluids and the Application to Separation Processes, Springer, 1994.

[27] Brunner G, Supercritical fluids: Technology and application to food processing, J Food Eng 67 (2005) 21–33.

[28] Wang J, Cui H, Wei S, Zhuo S, Wang L, Li Z and etc., Separation of biomass pyrolysis oil by supercritical CO_2 extraction, Smart Grid Renew Energy 1 (2010) 98–107.

[29] Goldfarb JL, Buessing L, Gunn E, Lever M, Billias A, Casoliba E and etc., Novel integrated biorefinery for olive mill waste management: utilization of secondary waste for water treatment, ACS Sust Chem Eng 5 (2017) 876–84.

[30] Schievano A, Adani F, Buessing L, Botto A, Casoliba EN, Rossoni M and etc., An integrated biorefinery concept for olive mill waste management: supercritical CO_2 extraction and energy recovery, Green Chem 17 (2015) 2874–87.

[31] Hakkila P, Utilization of residual biomass, Springer, 1989.

[32] Lestander TA, Lindeberg J, Eriksson D, Bergsten U, Prediction of Pinus sylvestris clear-wood properties using NIR spectroscopy and biorthogonal partial least squares regression, Can J Forest Research 38 (2008) 2052–62.

[33] Gustafsson G, Heartwood and lightwood formation in Scots pine - A physological approach. PhD thesis, Swedish University of Agricultural Sciences, 2001.

[34] Backlund I, Cost-effective Cultivation of Lodgepole Pine for Biorefinary Applications. PhD thesis, Swedish University of Agricultural Sciences, 2013.

[35] Koch P, Lodgepole pine in North America: Nonwood products characterization of tree parts, Forest Prod Soc, 1996.

[36] Werkelin J, Skrifvars BJ, Zevenhoven M, Holmbom B, Huppa M, Chemical forms of ash-forming elements in woody biomass fuels, Fuel 89 (2010) 481–93.

[37] Oasmaa A, Kuoppala E, Gust S, Solantausta Y, Fast pyrolysis of forestry residue. 1. Effect of Extractives on Phase Separation of Pyrolysis Liquids, Energy Fuels 17 (2003) 437–43.

[38] Myeong S, Han SH, Shin SJ, Analysis of Chemical Compositions and Energy Contents of Different Parts of Yellow Poplar for Development of Bioenergy Technology, J Korean For Soc 99 (2010) 706–10.

[39] Sluiter A, Hames B, Ruiz R, Scarlata C, Sluiter J, Templeton D et al., Determination of Structural Carbohydrates and Lignin in Biomass. Golden (CO): National Renewable Energy Laboratory; 2011 July Report No. NREL/TP-510-42618. Contract No.: DE-AC36-08-GO28308 (2010).

[40] Willför S, Hemming J, Leppänen AS, Analysis of extractives in different pulps - Method development, evaluation, and recommendations. Finland: Åbo Akademi University, Laboratory of Wood and Paper Chemistry; Report No. B1 of the EU COST E41 action "Analytical tools with applications for wood and pulping chemistry" (2004-2009).

[41] Hames B, Ruiz R, Scarlata C, Sluiter J, Sluiter A, Preparation of Samples for Compositional Analysis. Golden (CO): National Renewable Energy Laboratory; Report No. NREL/TP-510-42620. Contract No.: DE-AC36-99-GO10337 (2011).

[42] Thammasouk K, Tandjo D, Penner MH, Influence of Extractives on the Analysis of Herbaceous Biomass, J Agric Food Chem 45 (1997) 437–43.

[43] Griessacher T, Antrekowitsch J, Steinlechner S, Charcoal from agricultural residues as alternative reducing agent in metal recycling, Biomass bioenerg 39 (2012) 139–46.

[44] Riva L, Surup GR, Wang L, Nielsen HK, Fantozzi F, Bidini G and etc., Analysis of optimal temperature, pressure and binder quantity for the production of biocarbon pellet to be used as a substitute for coke, Appl energy 256 (2019) 1–16.

[45] ASTM D5373-02, Standard Test Methods for Instrumental Determination of Carbon, Hydrogen, and Nitrogen in Laboratory Samples of Coal and Coke. ASTM International (2016).

[46] ASTM D2216-19, Standard Test Methods for Laboratory Determination of Water (Moisture) Content of Soil and Rock by Mass. ASTM International (2016).

[47] ASTM D1102-84, Standard Test Method for Ash in Wood. ASTM International (2013).

[48] ASTM D3175-11, Standard Test Method for Volatile Matter in the Analysis Sample of Coal and Coke. ASTM International (2013).

[49] ASTM D3172-13, Standard Practice for Proximate Analysis of Coal and Coke. ASTM International (2013).

[50] ASTM D2015-95, Standard Test Method for Gross Calorific Value of Solid Fuel by the Adiabatic Bomb Calorimeter. ASTM International (1995).

[51] Behrens M, Datye AK, Methods for Biomass Compositional Analysis. In (ed. Schlögl R.): Catalysis for the Conversion of Biomass and Its Derivatives, Neopubli GmbH, 2013.

[52] Joffre T, Girlanda O, Forsberg F, Sahlén F, Sjödahl M, Gamstedt EK, A 3D in-situ investigation of the deformation in compressive loading in the thickness direction of cellulose fiber mats, Cellulose 22 (2015) 2993–3001.

[53] Forsberg F, Mooser R, Arnold M, Hack E, Wyss P, 3D micro-scale deformations of wood in bending: Synchrotron radiation μCT data analyzed with digital volume correlation, J Struct Biol 164 (2008) 255–62.

[54] Forsberg F, Sjödahl M, Mooser R, Hack E, Wyss P, Full Three-Dimensional Strain Measurements on Wood Exposed to Three-Point Bending: Analysis by Use of Digital Volume Correlation Applied to Synchrotron Radiation Micro-Computed Tomography Image Data, Strain 46 (2010) 47–60.

[55] Gamble JF, Terada M, Holzner C, Lavery L, Nicholson SJ, Timmens P and etc., Application of X-ray microtomography for the characterisation of hollow polymer-stabilised spray dried amorphous dispersion particles, Int J Pharma 510 (2016) 1–8.

[56] Otsu N, A Threshold Selection Method from Gray-Level Histograms, IEEE Transactions on systems, man, and cybernetics 9 (1979) 62–6.

[57] Plötze M, Niemz P, Porosity and pore size distribution of different wood types as determined by mercury intrusion porosimetry, Europ J Wood Wood Product 69 (2011) 649–57.

[58] Yin J, Song K, Lu Y, Zhao G, Yin Y, Comparison of changes in micropores and mesopores in the wood cell walls of sapwood and heartwood, Wood Sci Technol 49 (2015) 987–1001.

[59] Trubetskaya A, Poyraz Y, Weber R, Wadenbäck J, Secondary comminution of wood pellets in power plant and laboratory-scale mills, Fuel Process Tech 160 (2017) 216–27.

[60] Trubetskaya A, Beckmann G, Wadenbäck J, Holm JK, Velaga SP, Weber R, One way of representing the size and shape of biomass particles in combustion modeling, Fuel 206 (2017) 675–83.

[61] Umeki K, Bach-Oller A, Häggström G, Kirtania K, Furusjö K, Reduction of tar and soot formation from entrained-flow gasification of woody biomass by alkali impregnation, Energy Fuels 31 (2017) 5104–10.

[62] Bach-Oller A, Umeki K, Kirtania K, Furusjö K, Co-gasification of black liquor and pyrolysis oil at high temperature: Part 2. Fuel conversion, Fuel 197 (2017) 240–7.

[63] Trubetskaya A, Umeki K, Souihi N, Categorization of tars from fast pyrolysis of pure lignocellulosic compounds at high temperature, Renewable Energy 141 (2019) 751–9.

[64] R-Development-Core-Team, R: A Language and Environment for Statistical Computing, http://www.R-project.org/ (2011).

[65] Tolu J, Gerber L, Boily JF, Bindler R, High-throughput characterization of sediment organic matter by pyrolysis-gas chromatography/mass

spectrometry and multivariate curve resolution: A promising analytical tool in (paleo)limnology, Anal Chim Acta 880 (2015) 93–102.

[66] Gerber L, Eliasson M, Trygg J, Moritz T, Sundberg B, Multivariate curve resolution provides a high-throughput data processing pipeline for pyrolysis-gas chromatography/mass spectrometry, J Anal Appl Pyrolysis 95 (2012) 95–100.

[67] MS-SEARCH, NIST Mass Spectrometry Data Center: NIST/EPA/NIH Mass Spectral Database, http://chemdata.nist.gov (2011).

[68] Liu H, Xu L, Yan J, Fan B, Qiao X, Yang Y, Effect of coal rank on structure and dielectric properties of chars, Fuel 153 (2015) 249–56.

[69] Reyes T, Bandyopadhyay SS, McCoy BJ, Extraction of Lignin from Wood with Supercritical Alcohols, The J Supercrit Fluids 2 (1989) 80–4.

[70] Wong KKY, Deverell KF, Mackie KL, Clark TA, Donaldson LA, The relationship between fiber-porosity and cellulose digestibility in steam-exploded Pinus radiata, Biotech Bioeng 31 (1988) 447–56.

[71] Weber E, Fernandex M, Hoffman W, Wapner P, Comparison of X-Ray Micro-Tomography Measurements of Densities and Porosity to Traditional Techniques for Carbon-Carbon Composites, Defense Tech Inform Center, 2009.

[72] Erdogan ST, Simple Estimation of the Surface Area of Irregular 3D Particles, J Mat Civil Eng 28 (2016) 1–10.

[73] Hamdi SE, Delisee C, Malvestio J, Da Silva N, Le Duc A, Beaugrand J, X-ray computed microtomography and 2D image analysis for morphological chracterization of short lignocellulosic fibers raw materials: A benchmark survey, Composites: Part A 76 (2015) 1–9.

[74] Brewer CE, Chuang VJ, Masiello CA, Gonnermann H, Gao X, Dugan B and etc., New approaches to measuring biochar density and porosity, Biomass Bioenergy 66 (2014) 176–85.

[75] Moura MJ, Ferreira PJ, Figueiredo MM, Mercury intrusion porosimetry in pulp and paper technology, Powder Tech 160 (2005) 61–6.

[76] Zauer M, Hempel S, Pfriem A, Mechtcherine V, Wagenführ A, Investigations of the pore-size distribution of wood in the dry and wet state by means of mercury intrusion porosimetry, Wood Sci Technol 48 (2014) 1229–40.

[77] Wagenführ R, Holzatlas, Hanser, 2000.

[78] Schneider A, Wagner L, Bestimmung der Porengrößvenverteilung in Holz mit dem Quecksilber-Porosimeter, Holz Roh Werst 32 (1974) 216–24.

[79] Schneider A, Beitrag zur Porositätanalyse von Holz mit dem Quecksilber-Porosimeter, Holz Roh Werst 37 (1979) 295–302.

[80] Liese W, Fahnenbrock M, Elektromikroskopische Untersuchungen über den Bau der Hoftüpfel, Holz Roh Werkst 10 (1952) 197–201.

[81] Backlund I, Arshadi M, Hunt AJ, McElroy CR, Attard TM, Bergsten U, Extractive profiles of different lodgepole pine (*Pinus contorta*) fractions frown under a direct seeding-based silvicultural regime, Ind Crops Products 58 (2014) 220–9.

[82] Heupel RC, Sauvaire Y, Le PH, Parish EJ, Nes WD, Sterol composition and biosynthesis in sorghum: Importance to developmental regulation, Lipids 21 (1986) 69–75.

[83] Nes WR, Biochemistry of the Mevalonic Acid Pathway to Terpenoids, Plenum Press, 1990.

[84] Bell EA, Secondary Plant Products, Springer, 1980.

[85] Fischer C, Höll W, Free sterols, steryl esters, and lipid phosphorus in needles of scot's pine (Pinus sylvestris L.), Lipids 26 (1991) 934–9.

[86] Nes WR, Natural Products of Woody Plants II. Chemicals Extraneous to the Lignocellulosic Cell Wall, Springer, 1989.

[87] Höll W, Lipp J, Concentration gradients of free sterols, steryl esters and lipid phosphorus in the trunkwood of Scot's pine (Pinus sylvestris L.), Trees 1 (1987) 79–81.

[88] Saranpää P, Nyberg H, Lipids and sterols in Pinus sylvestris sapwood and heartwood, Trees 1 (1987) 82–7.

[89] Kumar M, Gupta RC, Industrial Uses of Wood Char, Energy Sources 20 (1998) 575–89.

[90] Russell NV, Beeley TJ, Man CK, Gibbins JR, Williamson J, Development of TG measurements of intrinsic char combustion reactivity for industrial and research purposes, Fuel Process Tech 57 (1998) 113–30.

[91] Trubetskaya A, Hofmann Larsen F, Shchukarev A, Umeki K, Ståhl K, Potassium and soot interaction in fast biomass pyrolysis at high temperatures, Fuel 225 (2018) 89–94.

[92] Atwater JE, Wheeler RR, Complex permittivities and dilectric relazation of granular activated carbons at microwave frequencies between 0.2 and 26 GHz, Carbon 41 (2003) 1801–7.

[93] Alias N, Zaini MAA, Kamaruddin MJ, Relationships between dielectric properties and characteristics of impregnated and activated samples of potassium carbonate- and sodium hydroxide-modified palm kernel shell for microwave-assisted activation, Carbon letters 24 (2017) 62–72.

[94] Ellison C, McKeown MS, Trabelsi S, Boldor D, Dielectric Properties of Biomass/Biochar Mixtures at Microwave Frequencies, Energies 10 (2017) 1–12.

[95] Solomon PR, Carangelo RM, FT-IR analysis of coal: 2. Aliphatic and aromatic hydrogen concentration, Fuel 67 (1988) 949–59.

[96] Selim MM, El-Nabarawy TA, Ghazy TM, Farid T, The relation between the adsorption characteristics of polar organic compounds (alcohols and acids) and their orientation polarization on activated carbon, Carbon 19 (1981) 161–5.

[97] Fornies-Marquina JM, Martin JC, Martinez JP, Miranda JL, Romero C, Dielectric characterization of coals, Can J Phys 81 (2003) 599–610.

[98] Ben AI, Arous M, Kallel A, Effect of maleic anhydride on dielectric properties of natural fiber composite, J Electrostat 72 (2014) 156–60.

[99] Shinoj S, Visvanathan R, Panigrahi S, Kochubabu M, Oil palm fiber (OPF) and its composites: a review, Ind Crops Prod 33 (2011) 7–22.

[100] Ramasamy S, Moghtaderi B, Dielectric Properties of Typical Australian Wood-Based Biomass Materials at Microwave Frequency, Energy Fuels 24 (2010) 4534–48.

[101] Sahin H, Ay N, Dielectric properties of hardwood species at microwave frequencies, J Wood Sci 50 (2004) 375–80.

[102] Masek O, Budarin V, Gronnow M, Crombie K, Brownsort P, Fitzpatrick E and etc., Microwave and slow pyrolysis biochar - Comparison pf physical and functional properties, J Anal Appl Pyrolysis 100 (2013) 41–8.

[103] Mumme J, Eckervogt L, Pielert J, Diakité M, Rupp F, Kern J, Hydrothermal carbonization of anaerobically digested maize silage, Biores Tech 102 (2011) 9255–60.

[104] Volpe M, Fiori L, From olive waste to solid biofuel through hydrothermal carbonization: The role of temperature and solid load on secondary char formation and hydrochar energy properties, J Anal Appl Pyrol 124 (2017) 63–72.

[105] Turton R, Bailie C, Whiting WB, Shaeiwitz JA, Analysis, Synthesis and Design of Chemical Processes, Prentice Hall, 2013.

[106] Rosa PTV, Meireles MAA, Rapid Estimation of the Manufacturing Cost of Extracts Obtained by Supercritical Fluid Extraction, J Food Eng 67 (2005) 235–40.

[107] De Melo MMR, Silvestre AJD, Silva CM, Supercritical fluid extraction of vegetable matrices: applications, trends and future perspectives of a convincing green technology, The J Super Fluids 92 (2014) 115–76.

[108] Attard TM, McElroy CR, Hunt AJ, Economic Assessment of Supercritical CO_2 Extraction of Waxes as Part of a Maize Stover Biorefinery, Int J Mol Sci 16 (2015) 17546–64.

[109] Deswarte FEI, Clark JH, Wilson AJ, Hardy JJE, Marriott R, Chahal SP, Jackson C and etc., Toward an integrated straw-based biorefinery, Biofuels, Bioprod and Bioref 1 (2007) 245–54.

[110] McElroy CR, Attard TM, Farmer TJ, Gaczynski D, Thornthwaite D, Clark JH and etc., Valorization of spruce needle waste via supercritical extraction of waxes and facile isolation of nonacosan-10-ol, J Clean Prod 171 (2018) 557–66.

[111] Vargas I, Sanz I, Moya P, Prima-Yufera E, Antimicrobial and Antioxidant Compounds in the Nonvolatile Fraction of Expressed Orange Essemtial Oil, J Food Protection 62 (1999) 929–32.

[112] Vargas I, Sanz I, Moya P, Prima-Yufera E, A New Diterpene with Antimicrobial Activity from Chamaecyparis pisifera Endle, Agricult Biolog Chem 42 (1978) 1419–23.

[113] Smith E, Williamson E, Zloh M, Gibbons S, Isopimaric acid from Pinus nigra shows activity against multidrug-resistant and EMRSA strains of Staphylococcus aureus, Phytother Res 19 (2005) 538–42.

[114] Fernandez MA, Tornos MP, Garcia MD, de las Heras B, Villar AM, Saenz MT, Anti-inflammatory activity of abietic acid, a diterpene isolated from pimenta racemosa var. grissea, J Pharm Pharmacol 53 (2001) 867–72.

[115] Ramani CC, Puranik PK, Dorle AK, Study of diabietic acid as matrix forming material, Int J Pharma 137 (1996) 11–9.

[116] Fulzele SV, Satturwar PM, Dorle AK, Study of the biodegradation and in vivo biocompatibility of novel biomaterials, Eur J Pharm Sci 20 (2003) 53–61.

[117] Bradford PG, Awad AB, Phytosterols as anticancer compounds, Mol Nutr Food Res 51 (2007) 161–70.